


5-31-2024

Electrochemical nitrate reduction to ammonia on Cu based nanoparticles using quantum mechanical simulations

Kathan Bhavin Shukla

New Jersey Institute of Technology, shuklakathan@gmail.com

Follow this and additional works at: <https://digitalcommons.njit.edu/theses>

 Part of the [Catalysis and Reaction Engineering Commons](#), and the [Other Materials Science and Engineering Commons](#)

Recommended Citation

Shukla, Kathan Bhavin, "Electrochemical nitrate reduction to ammonia on Cu based nanoparticles using quantum mechanical simulations" (2024). *Theses*. 2591.
<https://digitalcommons.njit.edu/theses/2591>

This Thesis is brought to you for free and open access by the Electronic Theses and Dissertations at Digital Commons @ NJIT. It has been accepted for inclusion in Theses by an authorized administrator of Digital Commons @ NJIT. For more information, please contact digitalcommons@njit.edu.

Copyright Warning & Restrictions

The copyright law of the United States (Title 17, United States Code) governs the making of photocopies or other reproductions of copyrighted material.

Under certain conditions specified in the law, libraries and archives are authorized to furnish a photocopy or other reproduction. One of these specified conditions is that the photocopy or reproduction is not to be “used for any purpose other than private study, scholarship, or research.” If a user makes a request for, or later uses, a photocopy or reproduction for purposes in excess of “fair use” that user may be liable for copyright infringement,

This institution reserves the right to refuse to accept a copying order if, in its judgment, fulfillment of the order would involve violation of copyright law.

Please Note: The author retains the copyright while the New Jersey Institute of Technology reserves the right to distribute this thesis or dissertation

Printing note: If you do not wish to print this page, then select “Pages from: first page # to: last page #” on the print dialog screen

The Van Houten library has removed some of the personal information and all signatures from the approval page and biographical sketches of theses and dissertations in order to protect the identity of NJIT graduates and faculty.

ABSTRACT

ELECTROCHEMICAL NITRATE REDUCTION TO AMMONIA ON CU BASED NANOPARTICLES USING QUANTUM MECHANICAL SIMULATIONS

by
Kathan Bhavin Shukla

Nitrate reduction to ammonia (NRA) is critical for environmental remediation and energy conservation, as it can remove harmful nitrate (NO_3^-) from water sources while producing usable ammonia (NH_3). Cu represents one of the most promising non-noble-metal NRA electrocatalysts. However, the intrinsic catalytic activity of Cu facets and their influence under different pH conditions remain unclear, particularly in the presence of ions commonly found in wastewater such as Cl^- , Na^+ , Mg^{2+} , and Ca^{2+} . Using density functional theory (DFT) calculations, we evaluated the nitrate reduction to ammonia (NRA) pathways on Cu(111), Cu(100), and Cu(110) surfaces across varying pH levels and contaminating ions. Our systematic thermodynamic and kinetic analysis revealed that proceeding through an $^*\text{NOH}$ intermediate is the most probable across all pH ranges. We observed that both the catalytic deoxygenation and hydrogenation processes in NRA are substantially affected by pH, and the presence of ions with pH- and ion-dependent rate-determining steps. Furthermore, we found that the presence of ions, especially Cl ions, enhances NO_3^- adsorption on all Cu facets. However, it influences the rate determining steps as well on each surface, with some steps, such as $^*\text{NO}$ to $^*\text{NOH}$ hydrogenation, becoming increasingly unfavorable.

Finally, we investigated NRA pathways on Cu-decorated Mxene surfaces to understand the effect of scaling Cu down to the atomic level. Cu functionalization of

Ti₂CO₂ MXene-lead to a significant increase in the NRA catalytic activity. These findings offer new strategies for the rational design of MXene-based NRA electrocatalysts with significance in environmental and energy-related applications.

**ELECTROCHEMICAL NITRATE REDUCTION TO AMMONIA ON CU BASED
NANOPARTICLES USING QUANTUM MECHANICAL SIMULATIONS**

**by
Kathan Bhavin Shukla**

**A Thesis
Submitted to the Faculty of
New Jersey Institute of Technology
in Partial Fulfillment to the Requirements for the Degree of
Master of Science in Chemical Engineering
Otto H. York Department of Chemical and Materials Engineering**

May 2024

APPROVAL PAGE

**ELECTROCHEMICAL NITRATE REDUCTION TO AMMONIA ON CU BASED
NANOPARTICLES USING QUANTUM MECHANICAL SIMULATIONS**

Kathan Bhavin Shukla

Dr. Joshua Young, Thesis Advisor	Date
Assistant Professor of Chemical and Materials Engineering, NJIT	

Dr. Xianqin Wang, Committee Member	Date
Professor of Chemical and Materials Engineering, NJIT	

Dr. Wen Zhang, Committee Member	Date
Professor of Civil and Environmental Engineering, NJIT	

BIOGRAPHICAL SKETCH

Author: Kathan Bhavin Shukla

Degree: Master of Science

Date: May 2024

Date of Birth:

Place of Birth:

Undergraduate and Graduate Education:

- Master of Science in Chemical Engineering,
New Jersey Institute of Technology, Newark, NJ, 2024
- Bachelor of Science in Chemical Engineering,
Ahmedabad University, Ahmedabad, India, 2018

Major: Chemical Engineering

This thesis is dedicated to the unwavering support and love of my parents, whose encouragement and sacrifices have been the cornerstone of my academic journey. Your belief in me has been my greatest strength, and I am forever grateful for your guidance and inspiration.

To my dear brother, Shalin, whose constant encouragement and understanding have been a source of motivation throughout this endeavor. Your presence in my life has been a constant source of joy, and I dedicate this work to you with heartfelt appreciation.

ACKNOWLEDGEMENTS

I wish to extend my heartfelt appreciation to Dr. Joshua Young, my thesis advisor, for his consistent support and guidance during the research process. His insightful feedback and invaluable comments have greatly contributed to the success of this thesis.

I am also deeply grateful to the members of my thesis committee, namely Dr. Xianquin Wang, and Dr. Zhang Wen, for their constructive criticism and valuable feedback.

I am indebted to the Chemical and Materials Engineering department for their financial assistance throughout my studies. Their generous support enabled me to focus entirely on my research, alleviating any financial constraints, for which I am sincerely thankful.

Furthermore, I am grateful to my colleagues and friends for their encouragement and intellectual exchange, which has been immensely beneficial.

Lastly, I am thankful to my family for their unwavering support and encouragement throughout my academic journey. Their love and support have been my greatest source of strength.

TABLE OF CONTENTS

Chapter	Page
1 INTRODUCTION	1
1.1 Background Information	1
1.1.1 Consequences of Nitrate Pollution	1
1.1.2 Importance of Nitrate Reduction to Ammonia	1
1.1.3 Catalysts for Nitrate Reduction	4
1.2 Purpose of the Study	6
2 LITERATURE REVIEW	7
2.1 Electrochemical Nitrate Reduction Mechanisms	7
2.1.1 Fundamental Components Consideration	8
2.2 Factors Influencing on Reaction Mechanism	11
2.3 Unexplored Aspects of NRA	12
2.3.1 Need for Computational Studies	13
3 METHODOLOGY	15
3.1 Density Functional Theory (DFT)	15
3.2 Computational Methods	16
3.3 Model Development	19
4 RESULTS & DISCUSSION	23
4.1 Nitrate Reduction to Ammonia on Cu Surfaces	23
4.1.1 NRA on Cu (001) Surface	23
4.1.2 NRA on Cu (110) Surface	26

TABLE OF CONTENTS (Continued)

Chapter	Page
4.1.3 NRA on Cu (111) Surface	29
4.2 Discussion and Comparison of NRA Performance on Cu Surfaces	32
4.3 NRA on Single Atom Cu on Mxene Surfaces	36
5 CONCLUSION	38
6 REFERENCES	39

LIST OF TABLES

Table	Page
2.1 Fundamental Steps of NRA1	9
2.2 Fundamental Steps of NRA2	9
2.3 Fundamental Steps of NRA3	10
4.1 Adsorption Energy of Different Ions on the Three Cu Surfaces	33
4.2 Adsorption Energy of *NO ₃ ⁻ on the Mxene Surfaces	37

LIST OF FIGURES

Figure	Page
1.1 Ammonia synthesis concept cycle from waste nitrates	1
3.1 Convergence of total energy with respect to plane wave energy cutoff (ENCUT) value	18
3.2 Convergence behavior of total energy as a function of the number of k-points	18
3.3 Configurations of most stable NO ₃ RR intermediates on Cu(001) (color notation: blue = Cu, red = O, silver = N, white = H)	20
3.4 Configurations of most stable NO ₃ RR intermediates on Cu(110) (color notation: blue = Cu, red = O, silver = N, white = H)	21
3.5 Configurations of most stable NO ₃ RR intermediates on Cu(111) (color notation: blue = Cu, red = O, silver = N, white = H)	21
3.6 Illustration of adsorbed NO ₃ ⁻ only on Cu(001) surface under influence of a) Cl ⁻ , b) Na ⁺ , and c) Mg ²⁺	22
4.1 The Gibbs free energies for different intermediates on Cu(001). Three kinds of pathways on Cu(001) at pH=0 present on (a) bare Cu, (b) in the presence of Cl ion, (c) in the presence of Na ion, and (d) in the presence of Mg ion	24
4.2 Illustrates the influence of various pH levels on the three pathways of NRA on the Cu(001) surface on (a) bare Cu, (b) in the presence of Cl ion, (c) in the presence of Na ion, and (d) in the presence of Mg ion . . .	25
4.3 The Gibbs free energies for different intermediates on Cu(110) are depicted. Three kinds of pathways on Cu(110) at pH=0 are presented: (a) on the bare Cu, (b) in the presence of Cl ion, (c) in the presence of Na ion, and (d) in the presence of Mg ion	28
4.4 Influence of varying pH levels on the three pathways of NRA on the Cu(110) surface on (a) bare Cu, (b) in the presence of Cl ion, (c) in the presence of Na ion, and (d) in the presence of Mg ion . . .	28
4.5 The Gibbs free energies for different intermediates on Cu(111). Three kinds of pathways on Cu(111) at pH=0 are presented: (a) on bare Cu, (b) in the presence of Cl ion, (c) in the presence of Na ion, and (d) in	29

LIST OF FIGURES (Continued)

Figure		Page
	the presence of Mg ion	
4.6	pH influences all three NRA pathways on Cu(111) surface on (a) bare Cu, (b) in the presence of Cl ion, (c) in the presence of Na ion, and (d) in the presence of Mg ion	31
4.7	Total density of states (DOS) of N, O, Cl, and Cu on (a) Cu(100), (b) Cu(110), and (c) Cu(111)	34
4.8	Minimum energy path and activation barrier of elementary step $*\text{NH} + * \text{H} \rightarrow * \text{NH}_2$. TS stands for transition state	35
4.9	Minimum energy path and activation barrier of elementary step $*\text{NH} + * \text{H} \rightarrow * \text{NH}_2$ in the presence of Cl ion. TS stands for transition state . . .	35
4.10	Schematic of single Cu Mxene-based materials (a) $\text{Cu}@\text{Ti}_2\text{CO}_2$, (b) $\text{Cu}@\text{Ti}_2\text{CO}_2\text{-O}_v$, and (c) $\text{Cu}@\text{Ti}_2\text{COF-O}_v$	36

CHAPTER 1

INTRODUCTION

1.1 Background Information

Research on sustainable solutions to environmental remediation is rapidly expanding because of the growing concern over the complex interactions between nitrogen-containing substances and the environment. The increasing use of compounds containing nitrogen has turned this essential element for life into a source of environmental pollution worldwide and an energy dilemma.

1.1.1 Consequences of Nitrate Pollution

Nitrate (NO_3^-) contamination in water bodies arises primarily from agricultural runoff, industrial activities, and wastewater discharge. The accumulation of nitrates in aquatic environments can lead to eutrophication, causing algal blooms, oxygen depletion, and disruption of aquatic ecosystems [1]. Moreover, nitrate pollution poses serious health risks to humans. Excessive nitrate intake, primarily through contaminated drinking water and food sources, can result in methemoglobinemia (blue baby syndrome) in infants and adverse health effects in adults, including gastrointestinal disorders and certain types of cancer [2]. To address the challenges posed by nitrate pollution, various remediation strategies have been explored, including electrochemical methods for nitrate reduction. Electrochemical reduction of nitrate to ammonia represents a promising approach for both environmental remediation and sustainable ammonia synthesis.

1.1.2 Importance of Nitrate Reduction to Ammonia

Ammonia (NH_3) is one of the most common industrial chemicals, used in everything from plastics and medicines to textiles and agriculture. Ammonia (NH_3) is one of the most common industrial chemicals, used in the production of everything from plastics and medicines to textiles and agriculture. As an alternative to the energy-intensive Haber-Bosch process, electrocatalytic nitrogen reduction catalysts are becoming more popular due to their promise as next-generation energy carriers with high energy density and clean emissions (Figure 1.1).

The Haber-Bosch process of producing ammonia includes a high-temperature, high-pressure interaction between hydrogen (H_2) and nitrogen (N_2), which contributes to energy inefficiency and environmental degradation. This has led to an increasing amount of interest in electrocatalytic ammonia synthesis starting from N_2 and using water as a source of hydrogen. Breaking the N-N triple bond in nitrogen gas is a difficulty, though, and it is made worse by the interference of the competitive hydrogen evolution reaction (HER) which has an impact on Faradaic efficiency. Furthermore, there is a risk to public health when large volumes of nitrate leak into aquifers and surface water.

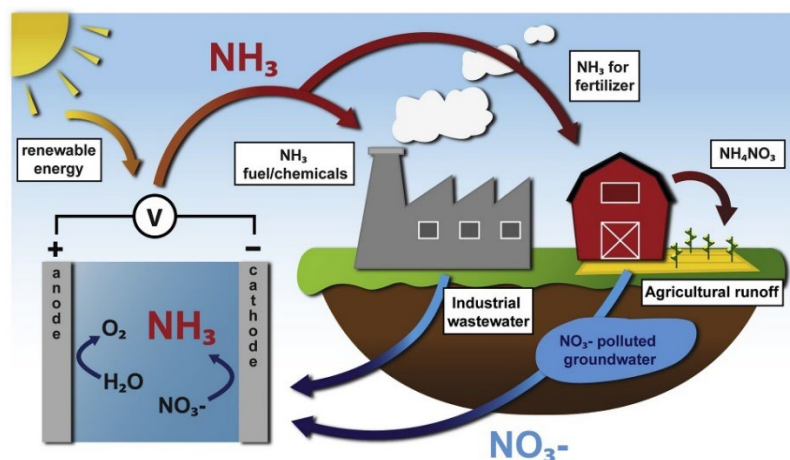


Figure 1.1 Ammonia Synthesis Concept Cycle from Waste Nitrates.

Source: Phebe H. van Langevelde, Ioannis Katsounaros, Marc T.M. Kope. (2021). Electrocatalytic Nitrate Reduction for Sustainable Ammonia Production. *Joule* 5, 290-294. [10.1016/j.joule.2020.12.025](https://doi.org/10.1016/j.joule.2020.12.025)

Instead of using N_2 with the strong N-N triple bond, an alternative approach is to use NO_3^- as feedstock, which contains weaker N-O bonds. Also, removing nitrate from wastewater is a critical process in environmental management, as excessive nitrate levels can lead to water pollution and ecosystem degradation. One commonly employed method for nitrate removal is biological denitrification. In this process, bacteria convert nitrate (NO_3^-) to nitrogen gas (N_2), which is then released harmlessly into the atmosphere. This biological approach is cost-effective and environmentally friendly, as it utilizes naturally occurring microorganisms to facilitate the conversion. However, biological denitrification requires careful control of environmental conditions, such as oxygen levels, pH, and temperature, to optimize bacterial activity. Additionally, it may not be suitable for treating wastewater with high nitrate concentrations or fluctuating flow rates, necessitating supplementary treatment methods [3].

Another method for nitrate removal is ion exchange, wherein nitrate ions are exchanged for other ions like chloride or sulfate on a resin surface. This process effectively removes nitrate from water but produces a concentrated nitrate solution that requires proper disposal. Furthermore, ion exchange can be expensive due to the need for resin regeneration or replacement [4]. Alternatively, chemical denitrification involves adding chemicals like sulfur-based compounds or iron salts to wastewater to convert nitrate to nitrogen gas or nitrous oxide. While effective, chemical denitrification can be costly and may introduce additional chemicals into the wastewater, requiring further treatment. Advanced oxidation processes, such as ozonation or UV irradiation, are emerging as promising techniques for nitrate removal, although they may also generate harmful byproducts and require careful monitoring [5].

In contrast to biological, chemical, and physical methods, electrochemical processes offer a promising avenue for nitrate removal from wastewater [6]. Electrochemical reduction of nitrate involves the application of an electrical current to drive a reaction that converts nitrate ions into harmless nitrogen gas or ammonia. In the case of nitrate reduction to ammonia (NH_3), the electrochemical process occurs at an electrode surface, typically made of materials like platinum, gold, or copper-based materials.

During the electrochemical reduction, nitrate ions (NO_3^-) are reduced at the cathode (negative electrode) while water molecules (H_2O) are simultaneously oxidized at the anode (positive electrode). At the cathode, nitrate undergoes a series of reduction steps, ultimately forming ammonia. The generated ammonia can then be recovered from the solution for further use or removed by appropriate downstream treatment processes. Electrochemical nitrate reduction offers several advantages, including high selectivity towards the desired end-product (ammonia), energy efficiency, and the ability to operate under ambient conditions without the need for high temperatures or pressures. Moreover, electrochemical systems can be easily integrated into existing wastewater treatment infrastructure, making them potentially cost-effective solutions for nitrate removal. However, challenges such as electrode fouling, scaling, and the need for efficient catalysts still need to be addressed to optimize the performance and scalability of electrochemical nitrate reduction technologies. Overall, electrochemical reduction holds significant promise as a sustainable and efficient method for addressing nitrate pollution in wastewater streams.

1.1.3 Catalysts for Nitrate Reduction

Transition metals play a crucial role as efficient electrocatalysts for the electrochemical reduction of nitrate (NO₃RR). Experimental studies have demonstrated the effectiveness of transition metals in promoting NO₃RR, with platinum group metals emerging as some of the most active materials for this purpose. Among the platinum group metals, rhodium (Rh), ruthenium (Ru), iridium (Ir), palladium (Pd), and platinum (Pt) exhibit varying degrees of activity towards NO₃RR, with the activity sequence in acidic media being Rh > Ru > Ir > Pd > Pt [7].

Interestingly, these metals exhibit high selectivity towards different nitrogen-containing products depending on the applied overpotential. Specifically, they demonstrate high selectivity to nitrous oxide (N₂O) at high overpotentials, nitrogen gas (N₂) at intermediate overpotentials, and ammonia (NH₃) at low overpotentials.

Furthermore, coinage metals such as copper (Cu), silver (Ag), and gold (Au) have also been investigated as electrocatalysts for NO₃RR [8], but metals generally exhibit lower activity compared to platinum group metals. However, Cu stands out for its relatively high activity, especially in acidic media. Due to its high activity and relatively low cost, Cu has garnered significant attention as an electrocatalyst for NO₃RR. Like Pt group metals, Cu demonstrates diverse distributions of intermediates and products under different reaction conditions, highlighting the complexity of the NO₃RR mechanism on copper surfaces.

In this context, the use of Cu-based catalysts holds promise for enhancing the efficiency and selectivity of the electrochemical reduction of nitrate to valuable nitrogen-containing compounds, such as ammonia.

Additionally, in electrochemical nitrate reduction, the presence and concentration of ions have a significant impact on the catalyst selection [9]. The system's charge transfer barrier may rise during wastewater treatment, particularly in circumstances involving low conductivity. There can be monetary losses as a result. Reaction paths and product concentrations are greatly influenced by the cation selection process because cations can modify surface characteristics to speed up reactions [10]. While Na^+ supports the creation of N_2O , the presence of K^+ encourages the formation of N_2 as the major product [11]. Thus, determining reaction paths and product concentrations greatly depends on the choice of cation. Like this, anions in the electrolyte solution affect electrostatic hindrance effects or compete for adsorption sites, which in turn affects catalytic effectiveness. For example, Cl^- influences the catalytic process overall by interacting with the anode to enhance reaction selectivity [8].

1.2 Purpose of the Study

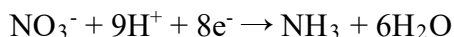
The purpose of this thesis is to explore the origin and functionality of an electrocatalyst based on Cu for the NRA reaction, thereby highlighting the complex mechanisms involved in nitrate adsorption and reduction on Cu surfaces. Investigating catalysts, such as Cu alloys, altered surfaces, and new materials, presents a viable path toward attaining sustainable ammonia production. By concentrating on comprehending the mechanistic elements and optimizing intermediate adsorption, this study advances the more general objective of tackling the worldwide issues brought about by nitrate contamination and energy-dense ammonia production.

CHAPTER 2

LITERATURE REVIEW

2.1 Electrochemical Nitrate Reduction Mechanisms

It is important to investigate and comprehend the mechanism of the electrochemical reduction of nitrate to ammonia (NRA) reaction, which entails complicated electron transfer and paths. The major products of nitrate reduction are thermodynamically stable N_2 and NH_3 , but there are many other complicated compounds that can be produced. From a kinetics standpoint, the process of reducing NO_3^- to NH_3 involves the transfer of eight-electrons. The overall NRA reaction proceeds as:



Adsorbed hydrogen reacts with adsorbed NO_3RR^- intermediates and NO_3^- dissociation products in the NO_3RR^- mechanism. The reaction pathway proceeds in more detail as follows. $*NO_3^-$ is created when the catalyst's surface absorbs NO_3^- from the solution, and $*NO_2$ is created when N-O is cracked. Additionally, further deoxygenation yields $*NO$; these direct deoxygenation steps were shown to be more favorable than hydrogenation (e.g. $*NO_2 + H^+ + e^- \rightarrow NO_2 + H_2O$). $*NO$ is subsequently hydrogenated to eventually produce NH_3 . Computationally, investigating the thermodynamics of the intermediates making up the reaction can lead to an understanding of the NRA pathway. The literature describes three different NRA pathways on Cu.

The first electrochemical mechanism proposed [12] is first a series of deoxidation reactions, where $*NO_3 \rightarrow *NO_2 \rightarrow *NO \rightarrow *NOH \rightarrow *N$, and then subsequent hydrogenation reactions, where $*N \rightarrow *NH \rightarrow *NH_2 \rightarrow *NH_3$, which is defined as NRA1. Tao Hu et al. (2021) have proposed two additional paths. The second is the process of $*NO_3 \rightarrow *NO_2 \rightarrow *NO \rightarrow *NOH \rightarrow *NHOH \rightarrow *NH_2OH \rightarrow *NH_2 \rightarrow *NH_3$, which forms NRA2 from the intermediate $*NOH$, $*NHOH$, and $*NH_2OH$. The third pathway is $*NO_3 \rightarrow *NO_2 \rightarrow *NO \rightarrow *NOH \rightarrow *NHOH \rightarrow *NH \rightarrow *NH_2 \rightarrow *NH_3$ and is called the NRA3 path. The reactions are different in that NRA1 goes through $*N$, whereas NRA2 goes through $*NHOH$. Furthermore, in NRA1 and NRA3, $*NH$ is an intermediate rather than $*NH_2OH$ in NRA2.

2.1.1 Fundamental Components Consideration

It is critical to fully understand the elementary processes involved in each of the three suggested NRA pathways, starting with the intermediates. The fundamental steps of each NRA are detailed in the three tables that are provided below. We note that these are reproduced from Tao Hu et al. (2021) [12].

Understanding both thermodynamics and kinetics is crucial for comprehensively studying the NRA process, especially when considering different pathways and the formation of various intermediates. Thermodynamics calculations provide insights into whether a particular pathway is energetically favorable (spontaneous) or not, and whether each intermediate will absorb or desorb. Considering different intermediates and pathways, thermodynamics can help predict which intermediates are likely to form and which pathways are more likely to be dominant under specific conditions.

Table 2.1 presents thermodynamic calculation steps which focus primarily on the overall energy changes associated with the reaction, particularly the change in Gibbs free energy. In kinetic calculations, the focus is on understanding the mechanisms and rates of individual elementary steps within the reaction mechanism by calculating energy barriers and transition states between steps. The notation used in the kinetic equations reflects the specific molecular interactions and bond formations and bond breaking involved in each step of the reaction mechanism.

Table 2.1 Fundamental Steps of NRA1

NRA1: $*NO_3^- \rightarrow *NO_2 \rightarrow *NO \rightarrow *NOH \rightarrow *N \rightarrow *NH \rightarrow *NH_2 \rightarrow *NH_3 \rightarrow NH_3(g)$	
Thermodynamics calculation	Kinetics calculation
$NO_3^- + * \rightarrow *NO_3 + e^-$	
$*NO_3 + 2H^+ + 2e^- \rightarrow *NO_2 + H_2O$	$*NO_3 \rightarrow *NO_2 + *O$ $*O + 2H^+ + 2e^- \rightarrow H_2O$
$*NO_2 + 2H^+ + 2e^- \rightarrow *NO + H_2O$	$*NO_2 \rightarrow *NO + *O$ $*O + 2H^+ + 2e^- \rightarrow H_2O$
$*NO + H^+ + e^- \rightarrow *NOH$	$*NO + *H \rightarrow *NOH$
$*NOH + H^+ + e^- \rightarrow *N + H_2O$	$*NOH \rightarrow *N$ $*OH + H^+ + e^- \rightarrow H_2O$
$*N + H^+ + e^- \rightarrow *NH$	
$*NH + H^+ + e^- \rightarrow *NH_2$	
$*NH_2 + H^+ + e^- \rightarrow *NH_3$	
$*NH_3 \rightarrow * + *NH_3 (g)$	

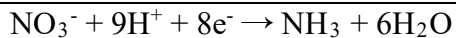


Table 2.2 Fundamental Steps of NRA2

NRA2: $*\text{NO}_3^- \rightarrow *\text{NO}_2 \rightarrow *\text{NO} \rightarrow *\text{NOH} \rightarrow *\text{NHOH} \rightarrow *\text{NH}_2\text{OH} \rightarrow *\text{NH}_2 \rightarrow *\text{NH}_3 \rightarrow \text{NH}_3 \text{ (g)}$	
Thermodynamics equation	Kinetics equation
$\text{NO}_3^- + * \rightarrow *\text{NO}_3 + \text{e}^-$	
$*\text{NO}_3 + 2\text{H}^+ + 2\text{e}^- \rightarrow *\text{NO}_2 + \text{H}_2\text{O}$	$*\text{NO}_3 \rightarrow *\text{NO}_2 + *\text{O}$ $*\text{O} + 2\text{H}^+ + 2\text{e}^- \rightarrow \text{H}_2\text{O}$
$*\text{NO}_2 + 2\text{H}^+ + 2\text{e}^- \rightarrow *\text{NO} + \text{H}_2\text{O}$	$*\text{NO}_2 \rightarrow *\text{NO} + *\text{O}$ $*\text{O} + 2\text{H}^+ + 2\text{e}^- \rightarrow \text{H}_2\text{O}$
$*\text{NO} + \text{H}^+ + \text{e}^- \rightarrow *\text{NOH}$	$*\text{NO} + *\text{H} \rightarrow *\text{NOH}$
$*\text{NOH} + \text{H}^+ + \text{e}^- \rightarrow *\text{NHOH}$	$*\text{NOH} + *\text{H} \rightarrow *\text{NHOH}$
$*\text{NHOH} + \text{H}^+ + \text{e}^- \rightarrow *\text{NH}_2\text{OH}$	$*\text{NHOH} + *\text{H} \rightarrow *\text{NH}_2\text{OH}$
$*\text{NH}_2\text{OH} + \text{H}^+ + \text{e}^- \rightarrow *\text{NH}_2 + \text{H}_2\text{O}$	$*\text{NH}_2\text{OH} + *\text{H} \rightarrow *\text{NH}_2 + \text{H}_2\text{O}$
$*\text{NH}_2 + \text{H}^+ + \text{e}^- \rightarrow *\text{NH}_3$	$*\text{NH}_2 + *\text{H} \rightarrow *\text{NH}_3$
$*\text{NH}_3 \rightarrow * + *\text{NH}_3 \text{ (g)}$	
$\text{NO}_3^- + 9\text{H}^+ + 8\text{e}^- \rightarrow \text{NH}_3 + 6\text{H}_2\text{O}$	

Table 2.3 Fundamental Steps of NRA3

NRA3: $*\text{NO}_3^- \rightarrow *\text{NO}_2 \rightarrow *\text{NO} \rightarrow *\text{NOH} \rightarrow *\text{NHOH} \rightarrow *\text{NH} \rightarrow *\text{NH}_2 \rightarrow *\text{NH}_3 \rightarrow \text{NH}_3 \text{ (g)}$
--

Thermodynamics equation	Kinetics equation
$\text{NO}_3^- + * \rightarrow *\text{NO}_3 + \text{e}^-$	
$*\text{NO}_3 + 2\text{H}^+ + 2\text{e}^- \rightarrow *\text{NO}_2 + \text{H}_2\text{O}$	$*\text{NO}_3 \rightarrow *\text{NO}_2 + *\text{O}$ $*\text{O} + 2\text{H}^+ + 2\text{e}^- \rightarrow \text{H}_2\text{O}$
$*\text{NO}_2 + 2\text{H}^+ + 2\text{e}^- \rightarrow *\text{NO} + \text{H}_2\text{O}$	$*\text{NO}_2 \rightarrow *\text{NO} + *\text{O}$ $*\text{O} + 2\text{H}^+ + 2\text{e}^- \rightarrow \text{H}_2\text{O}$
$*\text{NO} + \text{H}^+ + \text{e}^- \rightarrow *\text{NOH}$	$*\text{NO} + *\text{H} \rightarrow *\text{NOH}$
$*\text{NOH} + \text{H}^+ + \text{e}^- \rightarrow *\text{NHOH}$	$*\text{NOH} + *\text{H} \rightarrow *\text{NHOH}$
$*\text{NHOH} + \text{H}^+ + \text{e}^- \rightarrow *\text{NH} + \text{H}_2\text{O}$	$*\text{NHOH} + *\text{H} \rightarrow *\text{NH} + \text{H}_2\text{O}$
$*\text{NH} + \text{H}^+ + \text{e}^- \rightarrow *\text{NH}_2$	$*\text{NH} + *\text{H} \rightarrow *\text{NH}_2$
$*\text{NH}_2 + \text{H}^+ + \text{e}^- \rightarrow *\text{NH}_3$	$*\text{NH}_2 + *\text{H} \rightarrow *\text{NH}_3$
$*\text{NH}_3 \rightarrow * + *\text{NH}_3 (\text{g})$	
$\text{NO}_3^- + 9\text{H}^+ + 8\text{e}^- \rightarrow \text{NH}_3 + 6\text{H}_2\text{O}$	

2.2 Factors Influencing on Reaction Mechanism

The mechanism of NRA on Cu facets is influenced by various factors, including pH variation, the presence of different ions like Cl, Na, and Mg, and the specific Cu facet, such as, Cu (001), Cu (110), and Cu (111). pH plays a vital role in modulating surface chemistry and reactivity, with acidic conditions generally enhancing NRA rates due to increased surface protonation. Cl ions can compete with nitrate for surface adsorption, potentially inhibiting NRA pathways. Na ions indirectly influence NRA and the activity of Cu

surfaces, while Mg ions may compete with nitrate for adsorption and affect Cu surface activity.

The choice of Cu facet, such as Cu (001), Cu (110), and Cu (111), can significantly impact NRA rates due to variation in surface structure, coordination sites, and electronic properties. Therefore, understanding the interplay between these factors is crucial for predicting and controlling NRA on Cu facets in applications such as nitrate remediation or catalytic conversions.

2.3 Unexplored Aspects of NRA

Previous research has significantly advanced our understanding of the NRA reaction on Cu surfaces. Tao Hu et al. (2021) conducted a comprehensive study elucidating the electrocatalytic NRA process at different pH levels, revealing the NRA3 pathway as the most probable and thermodynamically favorable route on Cu surfaces [13]. Their work also highlighted the significance of surface morphology and local coordination environments in modulating NRA activity.

Building upon this, Wang et al. (2020) investigated the influence of pH variation on NRA using CuO nanowire arrays (NWAs), demonstrating excellent activity and selectivity for NRA [14]. They elucidated the electrochemical reconstruction of CuO NWAs to Cu/Cu₂O NWAs under reaction conditions, which played a crucial role in enhancing NRA efficiency. Furthermore, Yian et al. (2021) delved into the complex interactions between ions and Cu catalysts, particularly on Cu(100) and Cu(111) surfaces, using a hybrid DFT model [15]. Their findings revealed pH-dependent NRA pathways and highlighted the role of crystal facets in dictating NRA activity.

Despite these advancements, certain aspects remain unexplored, such as the combined impact of various ions present in wastewater and their synergistic or antagonistic effects on NRA pathways. Understanding these intricacies is essential for optimizing NRA processes and developing efficient nitrate remediation strategies tailored to real-world environmental conditions. Moreover, the influence of pH variation in the presence of ions represents another unexplored area in previous research on NRA. Dynamic changes in pH, coupled with the presence of ions, could significantly affect NRA rates and selectivity by altering surface charge, speciation of nitrate, and the availability of active sites on Cu catalysts.

Investigating the influence of pH under realistic ion-rich conditions is essential for comprehensively understanding NRA mechanisms and optimizing catalytic processes for nitrate removal. Furthermore, the impact of ions on NRA mechanisms may extend beyond simple competition for surface adsorption sites. Certain ions could potentially interact with Cu catalysts to form surface complexes or induce structural changes that alter the catalytic activity and selectivity towards NRA. Exploring these complex interactions between ions and Cu catalysts could uncover novel pathways and reaction mechanisms involved in NRA. By addressing these unexplored aspects, future research can advance our understanding of nitrate reduction processes in wastewater treatment and catalytic applications, ultimately leading to the development of more efficient and sustainable nitrate remediation technologies.

2.3.1 Need for Computational Studies

Computational studies, particularly Density Functional Theory (DFT), are crucial for exploring the unexplored aspects of nitrate reduction to ammonia (NRA) in the presence

of different ions and varying pH conditions. DFT calculations can provide detailed insights into the electronic structure, surface chemistry, and reaction mechanisms involved in NRA on Cu catalysts. By simulating complex interactions between ions and Cu surfaces at the atomic level, DFT allows to predict how these factors influence NRA pathways and selectivity. Moreover, computational studies can complement experimental observations, guiding the design of more effective catalyst and informing experimental investigations in a cost-effective and time-efficient manner.

CHAPTER 3

METHODOLOGY

3.1 Density Functional Theory (DFT)

Density Functional Theory (DFT) [16] serves as a powerful computational tool for unraveling the complex mechanisms underlying nitrate reduction to ammonia, facilitating the design of efficient catalysts and the optimization of reaction conditions for practical applications in environmental remediation and ammonia synthesis. Therefore, it is crucial for understanding and predicting the mechanisms involved in nitrate reduction to ammonia.

It allows for accurate calculations of the electronic structure of molecules and surfaces involved in nitrate reduction reactions. This includes determining the energies of the molecular orbitals, electron densities, and bond strengths, which are critical for understanding reaction mechanisms. By utilizing DFT, it can powerfully explore various reaction pathways involved in nitrate reduction to ammonia. This includes examining intermediate states, transition states, and energy barriers along the reaction coordinate, providing insights into the most favorable pathways and potential rate-limiting steps.

DFT is instrumental in the design and optimization of catalysts for nitrate reduction reactions. By simulating the interactions between catalyst surfaces and reactant molecules,

DFT can identify catalyst materials with favorable adsorption properties and catalytic activities, ultimately leading to the development of more efficient catalysts for ammonia production. Nitrate reduction reactions often occur on the surfaces of catalyst materials. DFT can elucidate the mechanisms of surface reactions, including adsorption, desorption, and surface intermediates formation. This understanding is crucial for engineering catalytic surfaces with enhanced reactivity and selectivity.

In my investigation of the nitrate reduction to ammonia, the utilization of DFT enables a comprehensive exploration of the underlying chemical mechanisms. Leveraging DFT, I have systematically elucidated the pathways of nitrate reduction, identified the rate-determining steps, and discerned optimal catalyst surfaces with enhanced activity. Furthermore, the DFT analysis has facilitated the thorough examination of additional factors, including pH variations and the influence of ions, providing comprehensive insights into the intricacies of the chemical processes involved.

3.2 Computational Methods

Spin-polarized density functional theory (DFT) calculations incorporating the Perdew-Burke-Ernzerhof (PBE) functional within the generalized gradient approximation (GGA) were conducted [16]. These calculations were executed employing the Vienna ab initio simulation package (VASP) [17]. The expansion of electronic eigenfunctions was described using the projector-augmented wave (PAW) [18] method with a kinetic energy cut-off of 700 eV. The thickness of slabs used in the study is at least four-layer atom thick. The convergence criteria for the electronic self-consistent loop and the Hellmann-Feynman forces on each atom were taken to be 10^{-6} eV [19]. All atomic positions were completely

relaxed until they met the energy and force convergence criteria, except for the lowest two surfaces of Cu. Solvation effects of water were considered using the VASPsol method [20], and Grimme's DFT-D3 method was integrated for van der Waals correction [21]. Charge variations were analyzed quantitatively using the Bader charge approach [22]. To obtain density of states (DOS) diagrams, VASPKIT [23] was employed as a pre- and post-processing tool for VASP.

Additional analysis was conducted focusing on the energy convergence testing for the plane wave energy cutoff (ENCUT) parameter using VASP for the Cu bulk and surface. We define the system and calculation parameters, focusing on a Cu crystal modeled using the PBE exchange-correlation function with a highly dense-centered Monkhorst-Pack k-point grid of 20x20x20. Starting at 500 eV, we set a range from 500 eV to 1000 eV for the ENCUT values. After collecting total energy values for each ENCUT, we analyze the results by plotting them against ENCUT to observe convergence visually. Figure 3.1 demonstrates that the energy converges as the ENCUT value increases, with diminishing changes in the total energy beyond an energy cutoff of 700 eV. Thereby, systematically determining the appropriate ENCUT value (700 eV) for our DFT calculations and ensuring reliable and accurate results for our material system.

For structural models of Cu (001), Cu (110), and Cu (111), a 5x5x1 supercell was adopted. Figure 3.2 illustrates the energy convergence with respect to the number of k-points sampled in the Brillouin zone for the different k-mesh configuration. This plot demonstrates that the chosen k-mesh size provides sufficient convergence, as evidenced by the plateauing of the energy as the number of k-points increases. Thus, the 5x5x1 k-mesh adequately captures the electronic structure and energetics of the system under study.

During relaxation, constraints were applied to certain axes, and a vacuum thickness of 20 Å was set to minimize interlayer interactions arising from the periodic boundary conditions.

The Gibbs free energy (ΔG) for each elementary step was calculated, using the energy from DFT calculations (ΔE), corrections for zero-point energy (ZPE) and entropy (S), and the effect of pH. The Gibbs free energy changes (ΔG) were calculated as the change in between two steps. The ZPE and S of each step was found by computing the vibrational spectrum of each intermediate on each Cu facet.

$$\Delta G = \Delta E + \Delta \text{ZPE} - T\Delta S + \Delta G_{\text{pH}}$$

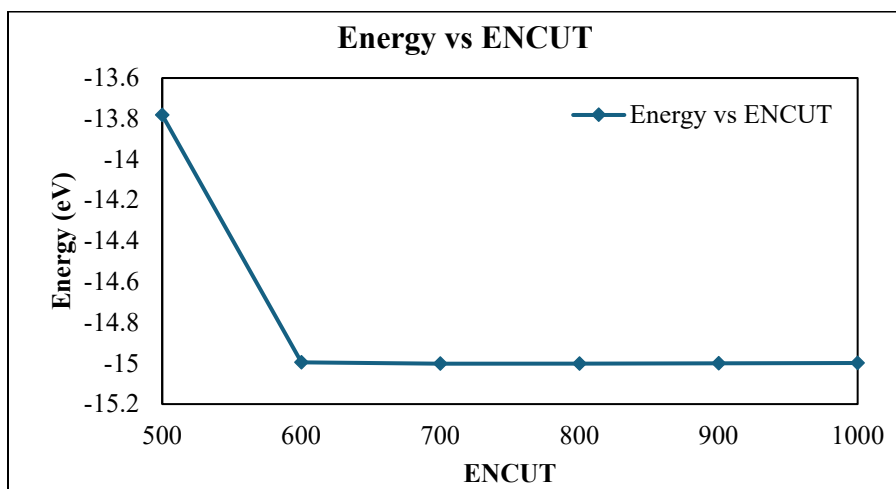


Figure 3.1 Convergence of total energy with respect to plane wave energy cutoff (ENCUT) value.

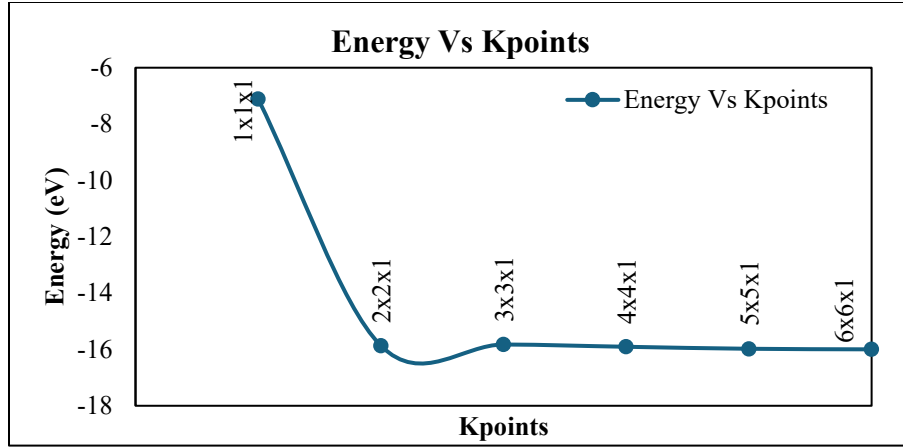


Figure 3.2 Convergence behavior of total energy as a function of the number of k-points. Room temperature $T = 298.15\text{K}$ is used in the calculation of ΔG to take temperature

into consideration. The adsorption energy of NO_3^- was described relative to gaseous NO_3H , with an applied 0.75 eV correction to compensate for the DFT calculation as described in Liu et al. (2019) [13]. The adsorption energy of NO_3^- ($\Delta G_{*\text{NO}_3}$) is therefore calculated as,

$$\Delta G_{\text{NO}_3} = E(*\text{NO}_3) + \frac{1}{2} E(\text{H}_2) - E(*) - E(\text{NO}_3\text{H}) + 0.75\text{ eV}$$

Where $E(*\text{NO}_3)$ is the total calculated energy from DFT of adsorbed NO_3^- , $E(\text{H}_2)$ is the total energy of a hydrogen molecule, minus the total energy of the clean Cu surface and nitric acid (NO_3H). At pH apart from 0, the free energies of reactions that H^+ takes part in are corrected by below equation.

$$\Delta G_{\text{pH}} = -k_{\text{B}}T \ln 10 \cdot \text{pH}$$

Where k_{B} is Boltzmann's constant, and T is temperature.

The climbing image nudged elastic band (CI-NEB) approach was utilized to determine minimum energy paths and activation barriers for elementary steps, with confirmation via frequency calculations [24].

3.3 Model Development

Here, we show how we found the intermediates on each surface corresponding to the computed energy-reaction diagrams presented in Chapter 4. The Cu (001), Cu (110), and Cu (111) surfaces were modeled as a 4x4 slab, 4x5 slab, and 5x5 slab, respectively. Four layers of Cu were selected to reduce the computational expense, being consistent with all three surfaces. The bottom two layers were fixed to simulate bulk, and the top two layers were fully relaxed. Each intermediate of each NRA pathway was then initialized on each Cu surface in different adsorption configurations, and the atomic positions were optimized. The lowest energy and most stable intermediate configurations on the Cu facets are depicted in the three figures below, with Cu(001) shown in Figure 3.3, Cu(110) shown in Figure 3.4, and Cu(111) shown in Figure 3.6.

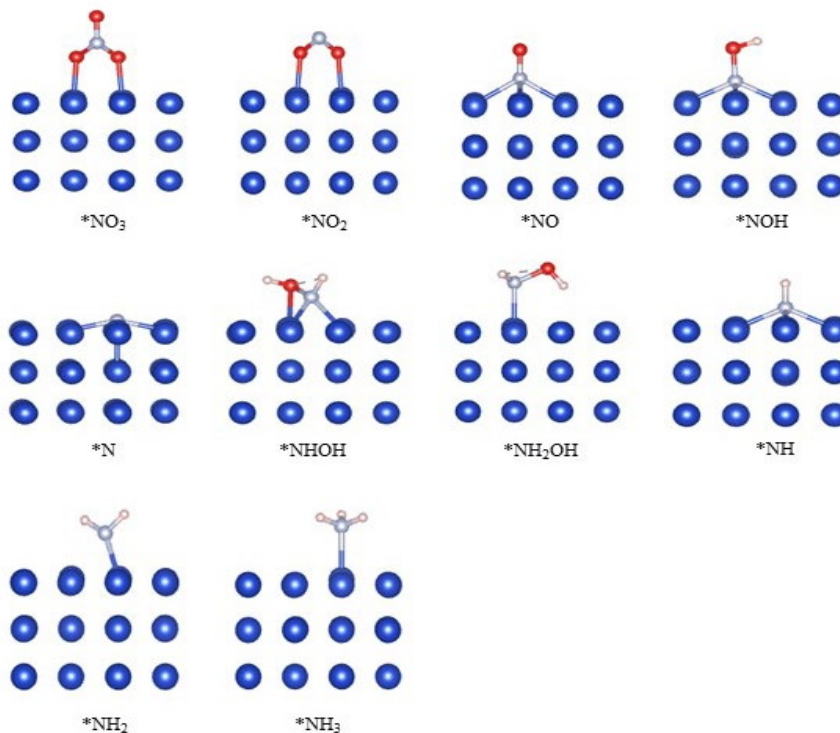


Figure 3.3 Configurations of most stable NO₃RR intermediates on Cu(001) (color notation: blue = Cu, red = O, silver = N, white = H).

Notably, the absorption of NO_3^- onto all three surfaces favored a chelating O,O-bidentate structure through two oxygen atoms, a mechanism supported by experimental evidence [25] and consistent with a previous theoretical investigations by Liu et al. (2019) [12]. The breaking of N-O bonds crucial for nitrate reduction is heavily influenced by this oxygen coordination. Furthermore, the impact of ions such as Cl^- , Na^+ , and Mg^{2+} on each intermediate species present on the three Cu surfaces was also modeled and is illustrated in Figure 3.5. Here, the corresponding ion was placed next to the intermediate, and the total energy recomputed by again fully optimizing the atomic positions.

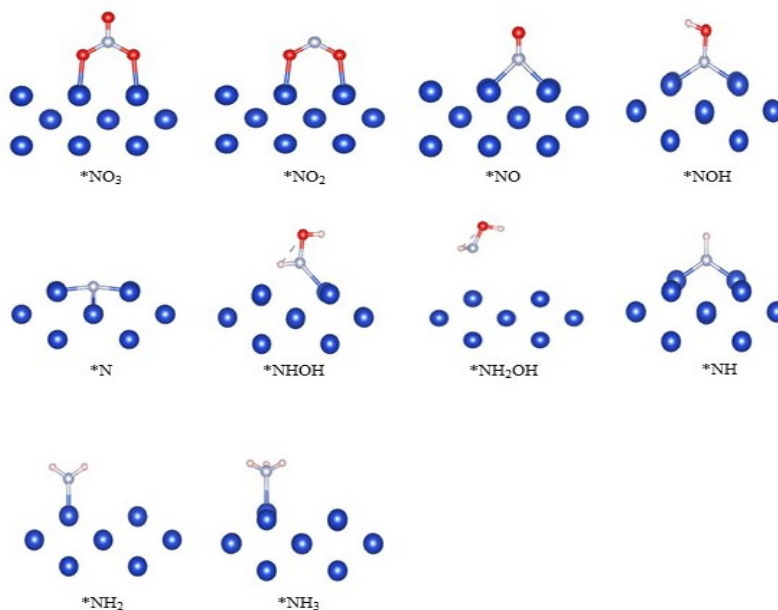


Figure 3.4 Configurations of most stable NO_3RR intermediates on $\text{Cu}(110)$ (color notation: blue = Cu, red = O, silver = N, white = H).

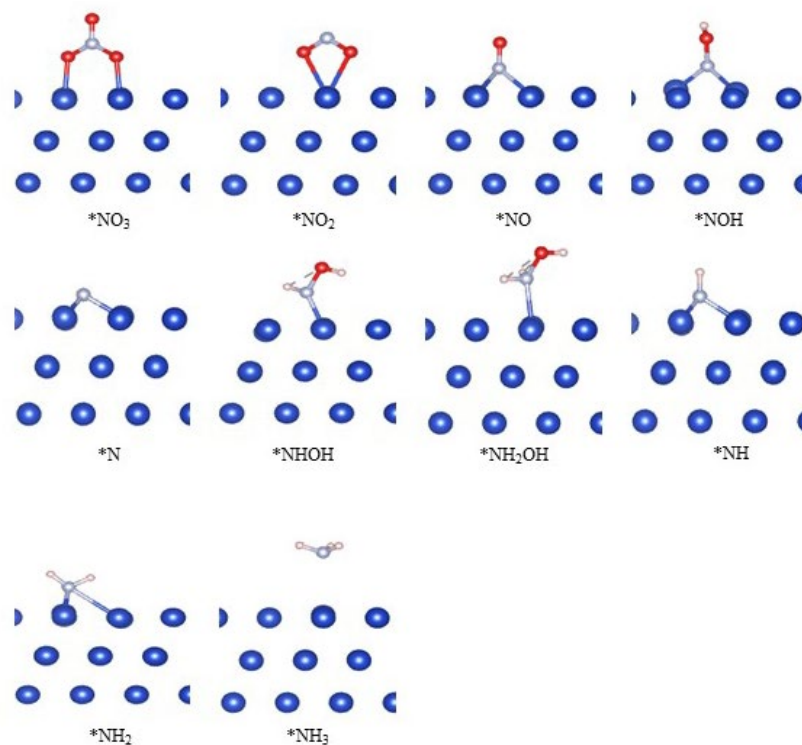


Figure 3.5 Configurations of most stable NO_3RR intermediates on Cu(111) (color notation: blue = Cu, red = O, silver = N, white = H).

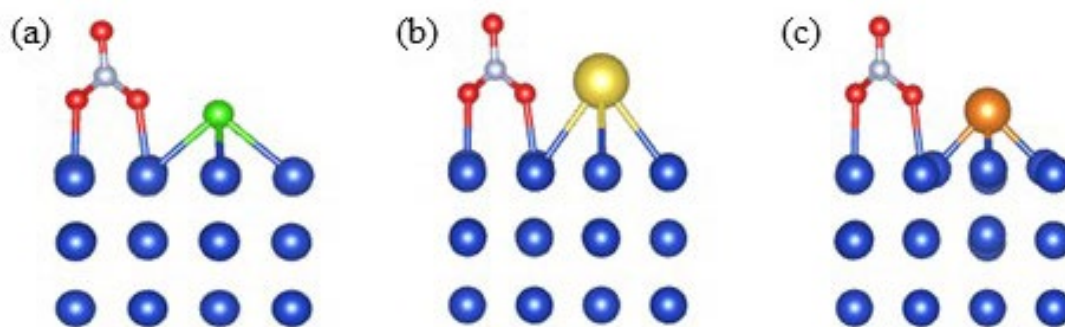


Figure 3.6 Illustration of adsorbed NO_3^- only on Cu (001) surface under influence of a) Cl^- , b) Na^+ , and c) Mg^{2+} .

CHAPTER 4

RESULTS & DISCUSSION

4.1 Nitrate Reduction to Ammonia on Cu Surfaces

This chapter describes a detailed explanation of three distinct NRA pathways observed on each Cu surface – Cu (001), Cu (110), and Cu (111). We also investigated the effects of pH and dissolved ions (Cl^- , Na^+ , and Mg^{2+}) on the NRA pathways. After that, we propose atomistic reasons for the observations using density of states and charge transfer calculations. Finally, we investigate the effect of reducing Cu to the atomic limit on nitrate

adsorption. Through thorough analysis and comparison, our aim is to offer valuable insights into how surface properties influence NRA mechanisms and product formation.

4.1.1 NRA on Cu (001) Surface

The Gibbs free energies of intermediates under working conditions play a pivotal role in determining reaction pathways. As such, all the energy reaction diagram of all 3 NRA pathways were evaluated on different Cu facets and in the presence of Cl^- , Na^+ , and Mg^{2+} , and under different pH conditions. These are shown in Figure 4.1 and 4.2 for Cu (001). First, the adsorption energy of NO_3^- on Cu (001) is found to be 0.15 eV on bare Cu. Positive adsorption energy indicates unfavorable adsorption. However, in the presence of ions, such as Cl^- , the adsorption of nitrate molecules on the Cu surface is significantly enhanced. Notably, in the presence of Cl^- ions, the adsorption energy of NO_3^- decreases to -1.22 eV, indicating a stronger binding of NO_3^- to the Cu (001) surface when Cl is present (Figure 4.1b). Consequently, a study was conducted to assess the impact of cations. It was observed that Na^+ and Mg^{2+} ions also enhance the adsorption of NO_3^- with an energy of -1.83 eV and -1.17 respectively. However, in this context, Na ions exhibit superior adsorption enhancement compared to Cl and Mg ions on the Cu (001) surface when it comes to binding NO_3^- molecules.

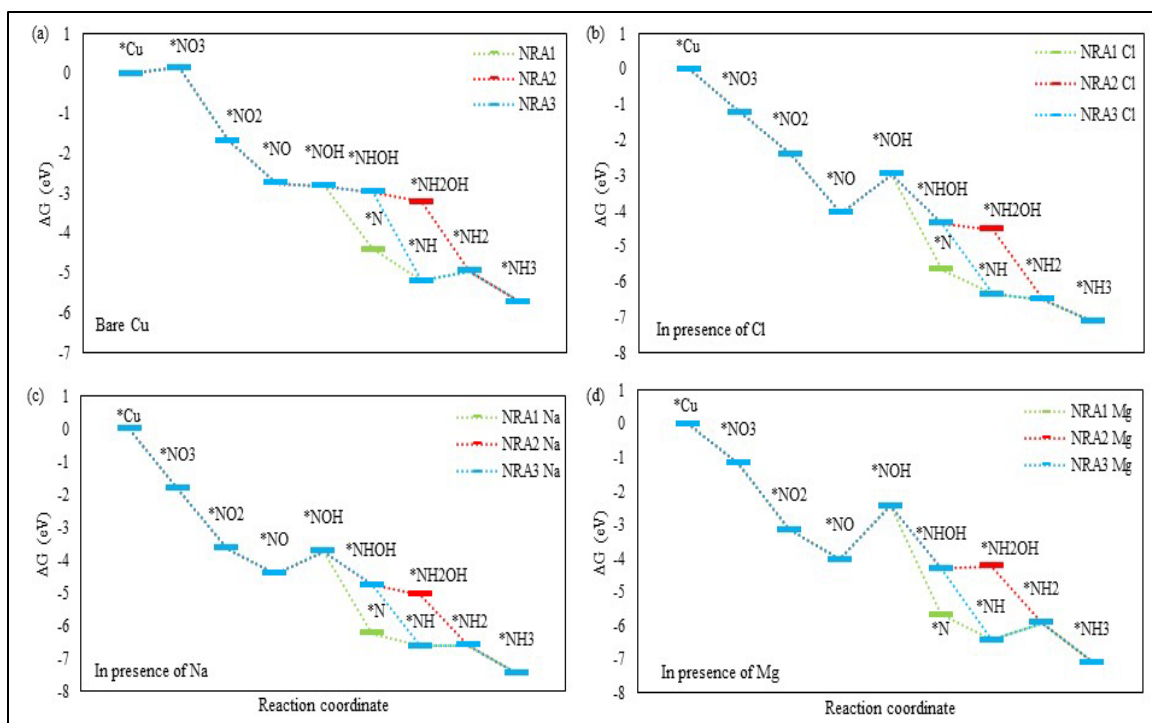


Figure 4.1 The Gibbs free energies for different intermediates on Cu(001). Three kinds of pathways on Cu(001) at pH=0 present on (a) bare Cu, (b) in the presence of Cl ion, (c) in the presence of Na ion, and (d) in the presence of Mg ion.

After adsorption, the Gibbs free energy goes downhill for all pathways on bare Cu (001) until $^*\text{NH}_3$ is produced (Figure 4.1a), indicating effective production of NRA via the NRA2 pathway. The rate-determining step for NRA2 appears to be the adsorption of $^*\text{NO}_3^-$ to $^*\text{NO}_3$. Conversely, in the case of NRA1 and NRA3, the energy trend parallels that of NRA2 except for the transition from $^*\text{NH}$ to $^*\text{NH}_2$. This step, requiring 0.24 eV, serves as the rate-determining step in NRA1 and NRA3. Thermodynamically, NRA2 proves more favorable than NRA1 and NRA3 in this scenario. However, a kinetic study by Tao Hu et al. (2021) suggests that transitioning from $^*\text{NHOH}$ to $^*\text{NH}_2\text{OH}$ entails a higher activation barrier compared to transitioning from $^*\text{NHOH}$ to $^*\text{NH}$.

Surprisingly, the reduction of nitrate ions down to $^*\text{NO}$ demonstrates significant improvement in the presence of ions (Figure 4.1b, 4.1c, and 4.1d). However, after that step

from $^*\text{NO}$ to $^*\text{NOH}$ becomes endothermic (unfavorable). As such, the transition from $^*\text{NH}$ to $^*\text{NH}_2$ does not appear to be the rate-determining step except in the case where a Mg ion is present, as evidenced by the downward trend in energy. The ions however do influence this $^*\text{NH}$ to $^*\text{NH}_2$ step, with Cl turning it from endothermic to exothermic, Na^+ lowering the energy barrier but remaining endothermic, and Mg^{2+} having little effect. Regardless, it seems that the rate-determining step for all three pathways remains consistent, namely the transition from $^*\text{NO}$ to $^*\text{NOH}$. This analysis seems to indicate that nitric oxide (NO) is likely to be a major product in the presence of dissolved ions under acidic (pH=0) conditions.

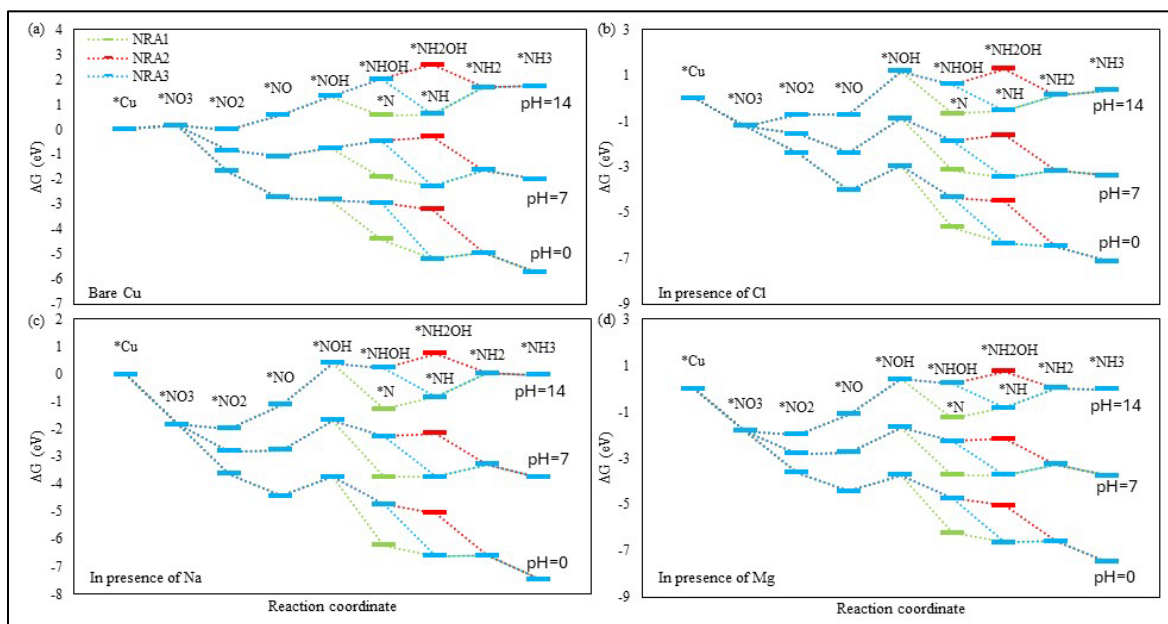


Figure 4.2 Illustrates the influence of various pH levels on the three pathways of NRA on the Cu(001) surface on (a) bare Cu, (b) in the presence of Cl ion, (c) in the presence of Na ion, and (d) in the presence of Mg ion.

We next applied a pH correction to the free energy to investigate this effect. Figure 4.2 represents the Gibbs free energy evolutions of three NRA pathways in acidic, neutral, and alkaline solutions (pH = 0, 7, and 14, respectively). Importantly, pH exerts a significant influence on NRA performance. As pH increases, the energies of intermediates rise due to

the more sluggish kinetics of H^+ . It is evident that NRA is energetically favorable in acidic media where H^+ is abundant. The pH results indicate that NRA2 is unfavorable under all conditions, whereas NRA3 demonstrates better performance across all pH levels due to its low overpotential requirement. On the bare Cu(001) and surface (Figure 4.2a), at pH=7 the NRA proceeds exothermically until $*NO$, at which point hydrogenation becomes unfavorable; all other steps are endothermic as well, leading to potentially increased competition of NH_3 production with NO . Another notable change observed at pH=14 is the high free energy requirement for the deoxygenation of $*NO_2$ to $*NO$, necessitating the dissociation of O from nitrite, meaning likely enhanced production of competitive $*NO_2$.

The effect of the ions remains much the same under pH=7 as pH=0, with exothermic steps until $*NO$ to $*NOH$, so the behavior should be similar under acidic and alkaline conditions. However, things are different under pH=14. In the presence of the Cl^- ions, the very first step $*NO_3$ to $*NO_2$ becomes endothermic, meaning the reaction is difficult to get started. The $*NO_3$ to $*NO_2$ is still exothermic at pH=14 with Na^+ and Mg^{2+} , but the $*NO_2$ to $*NO$ becomes uphill in energy under these pH conditions. Therefore, under alkaline conditions, all ions help $*NO_3$ adsorption, but while the NRA pathways are similar between Na^+ and Mg^{2+} and the bare Cu (001) surface, the Cl^- ion affects it in a negative way by inhibiting the formation of $*NO_2$.

4.1.2 NRA on Cu (110) Surface

Taking Cu(110) into consideration, we observed a recorded adsorption energy of 0.58 eV for NO_3^- on bare Cu, indicating weaker nitrate adsorption than on Cu(001). However, the presence of ions again notably amplifies the adsorption of NO_3^- on the surface. With the Cu(110) surface, the adsorption energy of NO_3^- improves to -1.5 eV in the presence of Cl

ion. Similarly, with the presence of Na^+ and Mg^{2+} the adsorption energy of NO_3^- also improves slightly to -1.27 and -0.72 eV respectively. Figure 4.3 elucidates the influence of ions on the Cu(110) surface.

The rate-determining step for all three pathways is $^*\text{NO}$ to $^*\text{NOH}$ on the bare Cu(110) surface in acidic condition. In this case, the hydrogenation step transition from $^*\text{NO}$ requires +0.78 eV, which is significantly high. This is different than Cu(001), where the step is downhill. While subsequent steps are downhill, this rate-determining step inhibits NRA. Moreover, neither Cl nor Na and Mg ions improve certain intermediate steps such as $^*\text{NO}$ to $^*\text{NOH}$ and $^*\text{NHOH}$ to $^*\text{NH}_2\text{OH}$. Considering these observations, opting for Cu(110) for the NRA process appears highly unlikely due to the unfavorable energy requirements and the limited influence of ions on critical intermediate steps.

Under the influence of pH, the energy of the steps tends to increase as the pH level rises. This phenomenon holds true for the Cu(110) surface as well. Under neutral conditions, the hydrogenation steps of NRA2 from $^*\text{NOH} \rightarrow ^*\text{NHOH} \rightarrow ^*\text{NH}_2\text{OH}$ remain relatively constant, indicating that NRA is not favorable for inhibition under these circumstances.

At pH=14, the hydrogenation steps from $^*\text{NH}$ to $^*\text{NH}_2$ exhibit a downward trend, while $^*\text{NO}_2$ to $^*\text{NO}$ requires additional energy. Therefore, acidic and alkaline environments tend to produce NO on Cu(110), while alkaline ones tend to produce NO_2 . The effect of the ions remains much the same as on Cu(001), with all of them, as on the bare (110) surface, producing NO under acidic and neutral environments and NO_2 under alkaline ones.

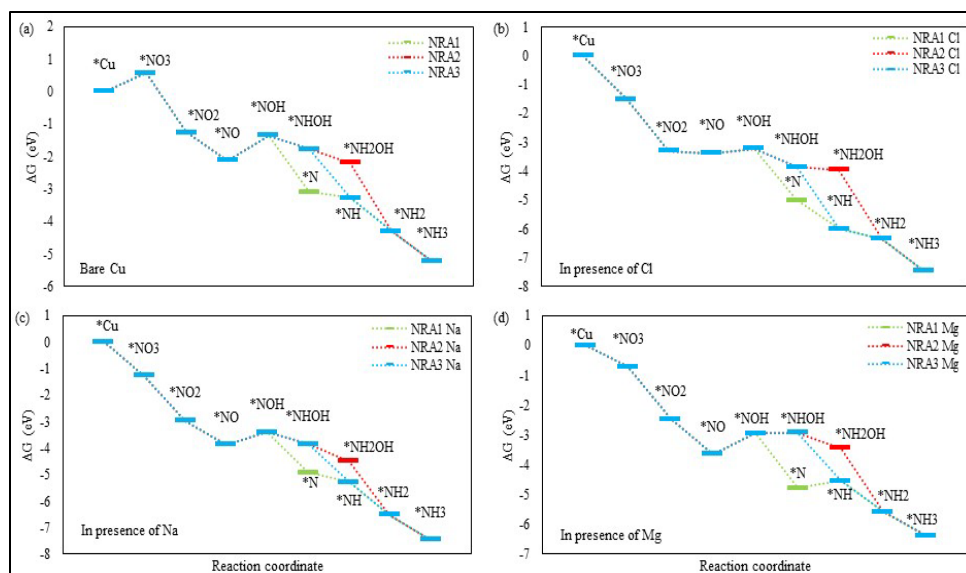


Figure 4.3 The Gibbs free energies for different intermediates on Cu(110) are depicted. Three kinds of pathways on Cu (110) at pH=0 are presented: (a) on bare Cu, (b) in the presence of Cl ion, (c) in the presence of Na ion, and (d) in the presence of Mg ion.

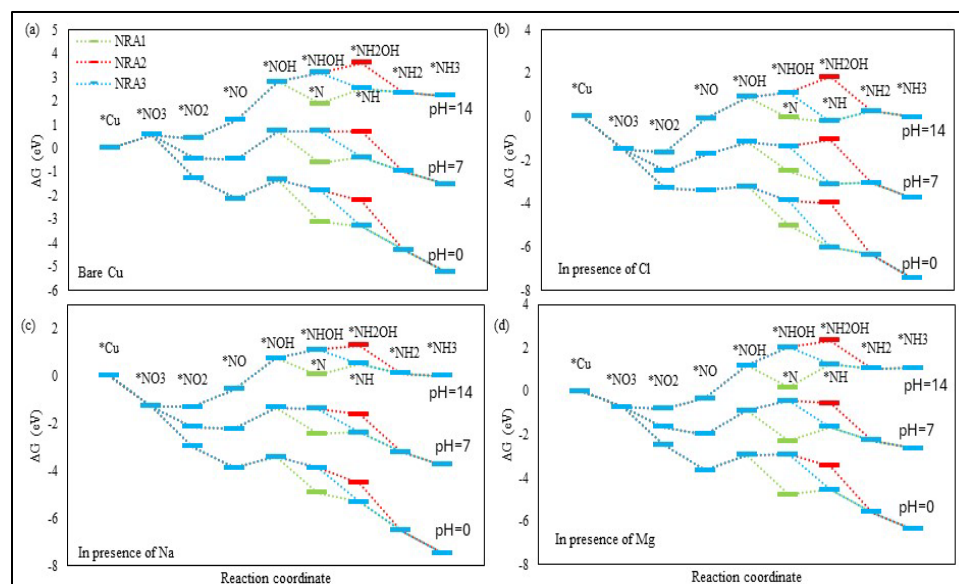


Figure 4.4 Influence of varying pH levels on the three pathways of NRA on the Cu (110) surface on (a) bare Cu, (b) in the presence of Cl ion, (c) in the presence of Na ion, and (d) in the presence of Mg ion.

4.1.3 NRA on Cu (111) Surface

The adsorption energy of NO_3^- on the Cu(111) surface is calculated to be 0.38 eV, potentially competitive with the Cu(001) surface. However, in terms of nitrate molecule

adsorption alone, the Cu(001) surface outperforms the Cu(111) surface. For this surface, all three pathways of NRA exhibit a downward energy trend following adsorption of nitrate. The sole uphill step is the hydrogenation of $^*\text{NO}$ to $^*\text{NOH}$, serving as the rate-determining step with a +0.86 -eV energy requirement. Thermodynamically analyzing the energy trends from Figure 4.5 suggests that NRA2 is not a suitable route for NRA reaction. The competition between NRA1 and NRA3 persists. Exploring other influencing factors for NRA, under Cl ion influence, $^*\text{N}$ formation proves more energetically favorable than $^*\text{NHOH}$ formation from $^*\text{NOH}$. This phenomenon stems from the release of water molecules during the $^*\text{NOH}$ step in NRA1. Conversely, in the presence of Na ions, both

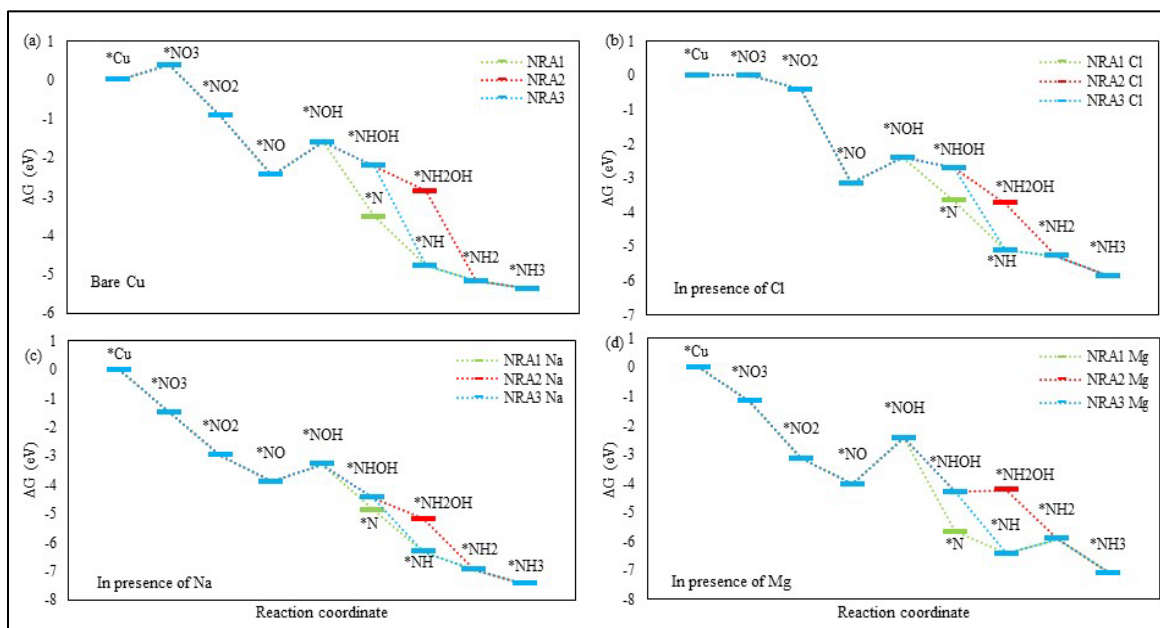


Figure 4.5 The Gibbs free energies for different intermediates on Cu(111). Three kinds of pathways on Cu(111) at pH=0 are presented: (a) on bare Cu, (b) in the presence of Cl ions, (c) in the presence of Na ions, and (d) in the presence of Mg ions.

$^*\text{N}$ and $^*\text{NHOH}$ exhibit nearly equal Gibbs free energy values. Another intriguing observation is that $^*\text{NO}_2$ to $^*\text{NO}$ is significantly more exothermic in the presence of Cl ions than in the presence of Na ions. However, both cation Na and Mg ions enhance the adsorption of nitrate ions, which is a positive aspect for NRA.

The Cu(111) surface is also influenced by various pH levels. In near-neutral conditions, the energy tends to increase compared to acidic environments. $^*\text{NH}_2$ exhibits an upward trend when transitioning from $^*\text{NH}$, then advancing to $^*\text{NH}_3$, with the energy rising by 0.20 eV. However, for other hydrogenation steps such as $^*\text{NHOH}$ to $^*\text{NH}_2\text{OH}$ and $^*\text{NOH}$ to $^*\text{NHOH}$, the trend is downward. Furthermore, with increasing pH, the energy shifts towards the more positive side, as observed in the previous two sections as well. Much of the same observation regarding product selectivity remains the same here, with one key difference. In the presence of Cl^- ions, now the reaction tends to do uphill at $^*\text{NO}_3$ to $^*\text{NO}_2$ under both neutral and alkaline conditions, whereas before this occurred under alkaline conditions only. Therefore, the inhibition of the NRA reaction is worse when Cl^- adsorbs to Cu(111) than Cu(001) or Cu(110).

To summarize, it is crucial to conduct a thermodynamic analysis of NRA pathways on Cu surfaces. As discussed in the preceding three sections, in acidic media on Cu(001), the potential-determining step (PDS) for NRA1 and NRA3 involves the reduction of $^*\text{NH}$ to $^*\text{NH}_2$ with a ΔG_{PDS} of 0.24 eV, while for NRA2, it is the adsorption of $^*\text{NO}_3$ with a ΔG_{PDS} of 0.15 eV. However, in the presence of Cl, Na, and Mg ions, the PDS for all three NRA pathways shifts to the reduction of $^*\text{NO}$ to $^*\text{NOH}$, with ΔG values of 1.08 eV, 0.68 eV, and 1.6 eV, respectively. Thermodynamically, Na ion would be a preferable choice for the NRA2 pathway on Cu(001) in acidic media. Similarly, in acidic media on Cu(111), the PDS for all NRA pathways would be the reduction of $^*\text{NO}$ to $^*\text{NOH}$, with Na also being preferable due to its lower ΔG_{PDS} value of 0.62 eV compared to Cl and Mg ions, which have ΔG_{PDS} values of 0.75 eV and 0.70 eV, respectively. Deciding the better-performing

NRA pathway based solely on Gibbs free energy becomes challenging; it necessitates kinetic analysis for each intermediate.

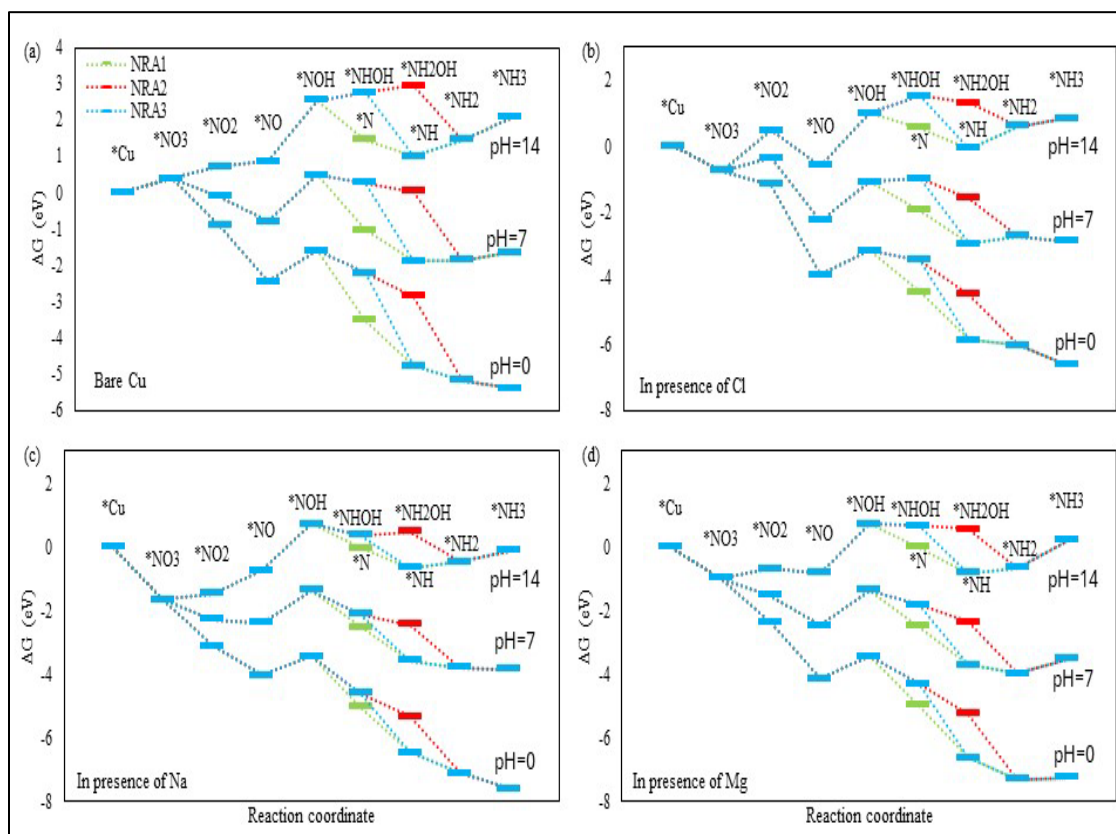


Figure 4.6 pH influences all three NRA pathways on Cu(111) surface on (a) bare Cu, (b) in the presence of Cl ion, (c) in the presence of Na ion, and (d) in the presence of Mg ion.

In alkaline media, Cu(001) inhibits *NO_2 , and subsequently, the reduction to *NO requires an overpotential of 0.59 eV on bare Cu. This remains consistent in the presence of cations, whereas in the presence of Cl ions, the formation of *NO_2 requires an overpotential of 0.48 eV. On bare Cu(111), the overpotential requirement from *NO_3^- to *NO_2 is 0.35 eV; however, in the presence of Na ions, it reduces to 0.19 eV, which is lower compared to Cl and Mg ions as well as bare Cu(111). Since the dominant NRA pathways and preferred Cu surfaces cannot be determined under these conditions, further analysis is warranted.

Overall, in the presence of Na ions, Cu(100) exhibits better performance than Cu(111) in acidic media, while the NRA pathways are yet to be decided.

4.2 Discussion and Comparison of NRA Performance on Cu Surfaces

The NRA performance on the three most typical surfaces, namely, Cu(111), Cu(001), and Cu(110), is compared. As mentioned in the previous sections, pH is shown to have a considerable influence on the free energies of intermediates. In acidic media, Cu(001) exhibits better NRA performance than Cu(111) and Cu(110) because of smaller positive NO_3^- adsorption energies. A similar trend is also observed when ions are present surrounding the adsorbed NO_3^- , as shown in Table 4.1. The adsorption energy of all three ions Cl, Na, and Mg are negative on the Cu surfaces, with Na^+ ions enhance the adsorption of nitrate the most. However, we find that ions themselves adsorb very strongly to the Cu surfaces, much more strongly than nitrate. Cl^- binds the strongest, followed by Na^+ , and then Mg^{2+} . This shows that while the ions actually help improve nitrate binding to the Cu surfaces, they can also inhibit it by competing for active sites. These two competing effects lead to the observation in Section 4.1.

Another study was conducted by computing the Density of States (DOS) to understand why nitrate binds more strongly on the three Cu surfaces in the presence of ions. Generally, Cu-based materials exhibit high potential in NO_3^- reduction due to the similarity in their d-orbital energy levels overlapping with the p-orbitals of oxygen. This phenomenon is evident in Figure 3.5, where the two O atoms of the NO_3^- ion bind with Cu atoms, resulting in the observed overlap of O p-states and Cu-d states shown in Figure 4.7a, 4.7b, and 4.7c, which illustrates the electronic states of N, O, Cl, Cu(001), Cu(110), and

Cu(111), respectively. The DOS graph of Cu(001) reveals that in the presence of Cl^- (Figure 4.7d), there is significant overlap between the O p-states of nitrate and p-states of Cl, indicating that Cl binds NO_3^- more strongly compared to when Cl is absent. A similar pattern was observed for the other two Cu surfaces as well (Figure 4.7e and 4.7f for (110) and (111), respectively). This helps indicate the reason Cl^- improves NO_3^- adsorption on the Cu surfaces.

Table 4.1 Adsorption Energy of Different Ions on the Three Cu Surfaces

Adsorption Energy (eV)			
Components	Cu surfaces		
	Cu (001)	Cu (110)	Cu (111)
Adsorption of *NO_3 on Cu surface (*NO_3)	0.152	0.582	0.385
Adsorption of *NO_3 in presence of Cl ion ($\text{*NO}_3\text{-Cl}$)	-1.217	-1.503	-0.749
Adsorption of *NO_3 in presence of Na ion ($\text{*NO}_3\text{-Na}$)	-1.827	-1.273	-1.651
Adsorption of *NO_3 in presence of Mg ion ($\text{*NO}_3\text{-Mg}$)	-1.165	-0.724	-0.983
Adsorption of Cl ion on Cu surface (*Cl)	-3.68	-3.72	-3.44
Adsorption of Na ion on Cu surface (*Na)	-1.56	-2.25	-1.88
Adsorption of Mg ion on Cu surface (*Mg)	-1.34	-1.75	-0.94
Adsorption of Cl ion when *NO_3 is present on Cu surface (*Cl- NO_3)	-3.68	-3.61	-3.27
Adsorption of Na ion when *NO_3 is present on Cu surface (*Na- NO_3)	-2.15	-1.89	-2.61
Adsorption of Mg ion when *NO_3 is present on Cu surface (*Mg- NO_3)	-1.73	-0.99	-1.27

Next, kinetic studies were conducted to further investigate and compare the reaction barriers on the Cu(111) surface with and without Cl influence. Specifically, considering the somewhat ambiguous thermodynamic results for Cu(111), kinetic studies became necessary and valuable in understanding the reaction mechanism, as depicted in Figures 4.8 and 4.9. Hence, kinetic barriers were calculated for the hydrogenation of $^*\text{NH}$ to $^*\text{NH}_2$, with configurations of the initial, transition, and final states shown in Figures 4.8 and 4.9.

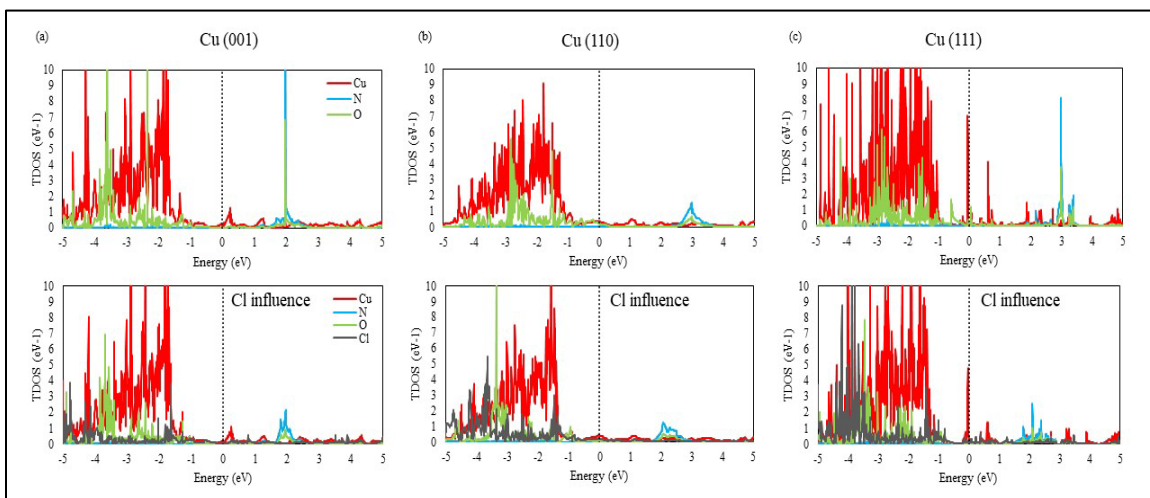


Figure 4.7 Total density of states (DOS) of N, O, Cl, and Cu on (a) Cu(001), (b) Cu(110), and (c) Cu(111).

For estimating barriers, since the proton source could be either water molecules in the solvent or adsorbed hydrogen on the surface, the kinetic energy barriers for the reduction of $^*\text{NH}$ were determined. When a proton is transferred directly from a nearby adsorbed $^*\text{H}$ proton to $^*\text{NH}$ to form $^*\text{NH}_2$, kinetic barriers of 0.67 eV (without Cl) and 0.92 eV (with Cl) were found, respectively. Consequently, the barrier under Cl influence was comparatively higher than without Cl influence. Thus, based on this study, assumptions can be made that for other intermediates of NRA, ions may exhibit a higher energy barrier compared to when no ions are present.

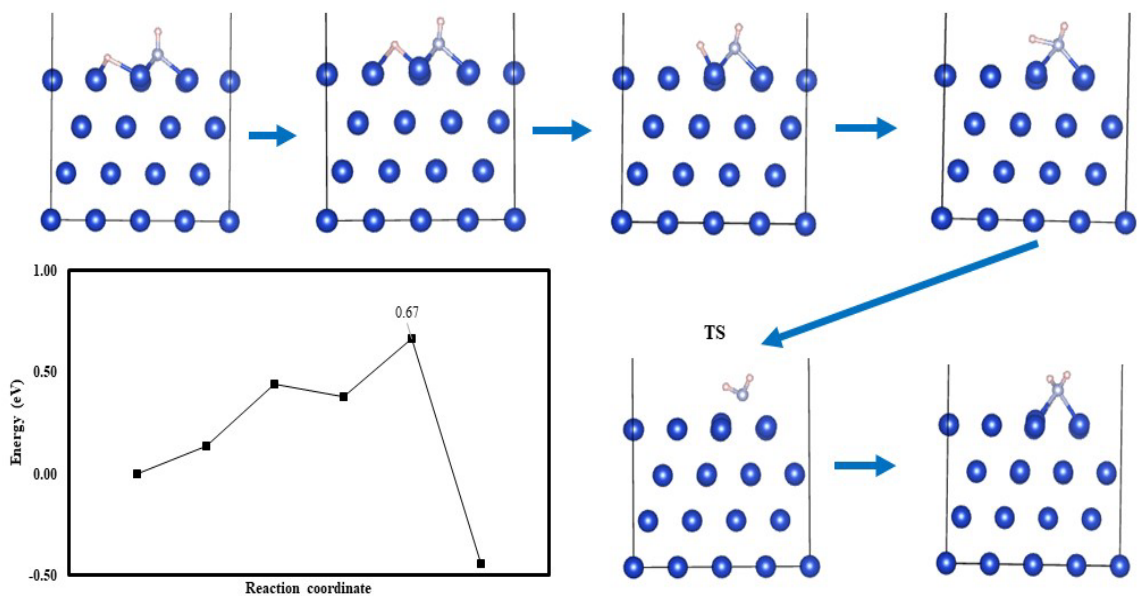


Figure 4.8 Minimum energy path and activation barrier of elementary step $*\text{NH} + * \text{H} \rightarrow * \text{NH}_2$. TS stands for transition state.

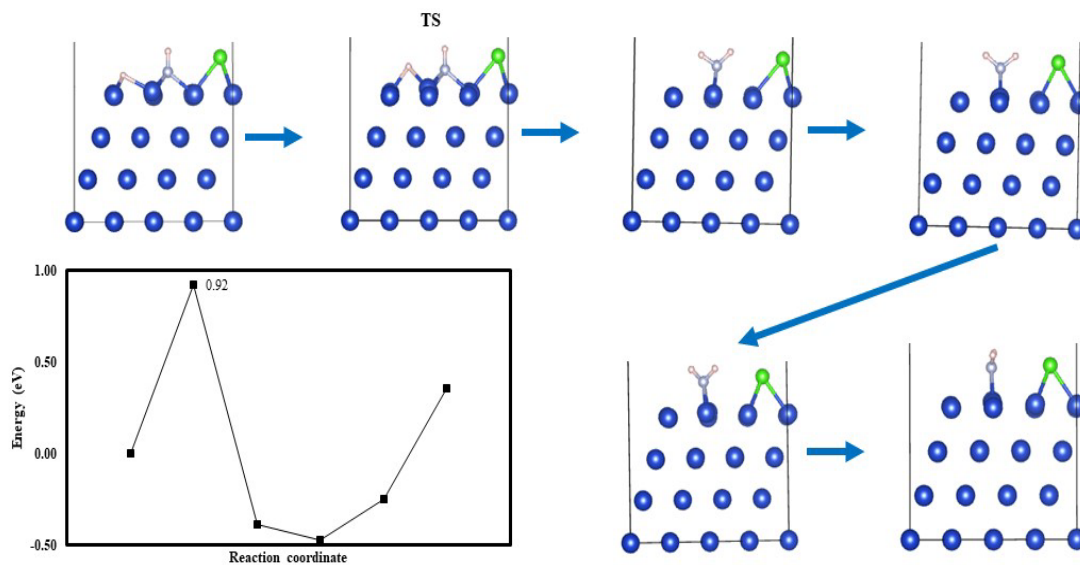


Figure 4.9 Minimum energy path and activation barrier of elementary step $*\text{NH} + * \text{H} \rightarrow * \text{NH}_2$ in the presence of Cl ion. TS stands for transition state.

4.3 NRA on Single Cu on Mxene Surfaces

As mentioned in the last section regarding the adsorption energy of $*\text{NO}_3^-$, a similar study has been conducted for Cu at the atomic limit, as well as the effect of different substrates.

In this investigation, Ti_2CX_2 ($\text{X} = \text{O}, \text{F}$) Mxenes with single Cu atoms was chosen for NO_3^- adsorption. Three types of Mxene surfaces, namely Ti_2CO_2 , $\text{Ti}_2\text{CO}_2\text{-O}_v$, and $\text{Ti}_2\text{COF-O}_v$ were simulated, where O_v indicates an O vacancy in the Mxene surface. Surface functionalization was introduced to enhance catalytic activity on the Mxene surfaces, which has been shown to have a large effect [26, 27]. Single Cu was subsequently added to the Mxene surfaces and examined for NO_3^- adsorption. Figure 4.10 offers insights into the structures of Mxene and the binding of $^*\text{NO}_3^-$.

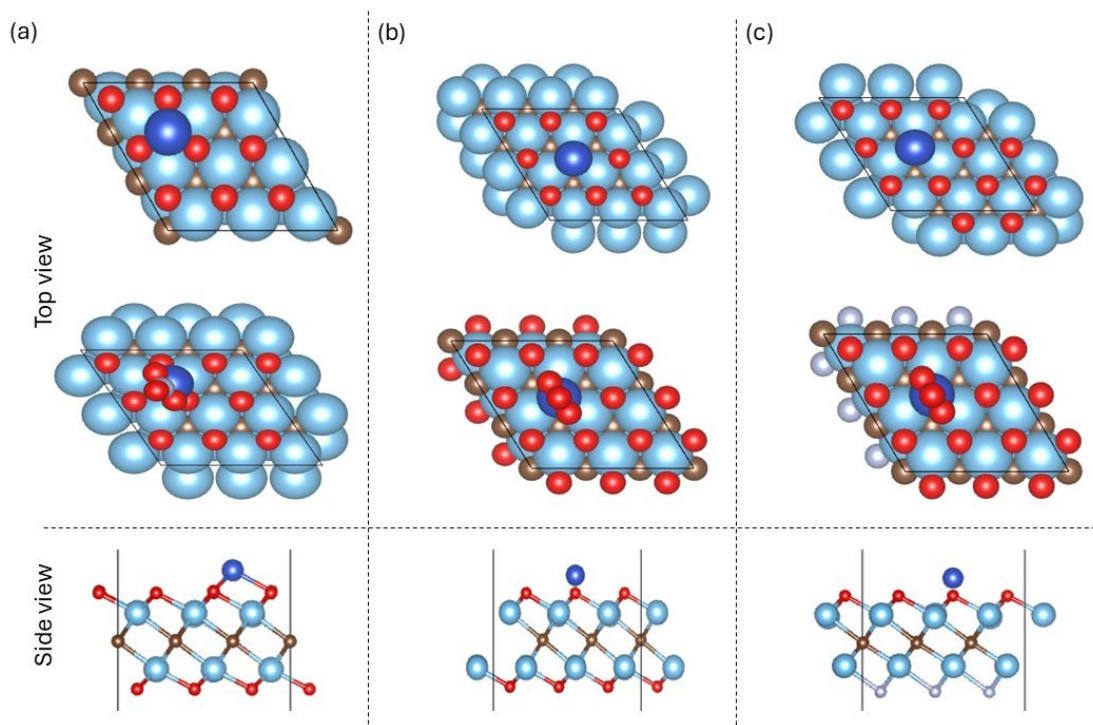


Figure 4.10 Schematic of single Cu Mxene-based materials (a) $\text{Cu@Ti}_2\text{CO}_2$, (b) $\text{Cu@Ti}_2\text{CO}_2\text{-O}_v$, and (c) $\text{Cu@Ti}_2\text{COF-O}_v$.

The adsorption energy of $^*\text{NO}_3^-$ on $\text{Cu@Ti}_2\text{CO}_2$ is the lowest among the three structures, at -0.68 eV. $\text{Cu@Ti}_2\text{CO}_2\text{-O}_v$ and $\text{Cu@Ti}_2\text{COF-O}_v$ also exhibit relatively low adsorption energies of -0.36 eV and -0.21 eV, respectively. The adsorption energy results indicate that $\text{Cu@Ti}_2\text{CO}_2$ binds $^*\text{NO}_3^-$ more strongly compared to others, as shown in Table 4.2. Moreover, when these surfaces are compared with the bare Cu surfaces $\text{Cu}(001)$,

Cu(110), and Cu(111), Mxene surfaces functionalized with Cu shows promising results when it comes to adsorption of $^*\text{NO}_3^-$.

Table 4.2 Adsorption Energy of $^*\text{NO}_3^-$ on the Mxene Surfaces

Surfaces	Adsorption Energy of $^*\text{NO}_3^-$ (eV)
Cu@Ti₂CO₂	-0.68
Cu@Ti₂CO₂-O_v	-0.36
Cu@Ti₂COF-O_v	-0.21

CHAPTER 5

CONCLUSION

In our investigation of the electrochemical reduction of nitrate to ammonia (NRA) on Cu surfaces using Density Functional Theory (DFT), we have uncovered crucial insights into the complex interplay between surface properties, surrounding ions, and reaction thermodynamics. Notably, Cu (001) emerges as a standout performer among the surfaces studied, exhibiting superior NRA efficiency. Interestingly, the presence of competing ions in the system manifests in dual effects: enhancing NO_3^- adsorption while significantly influencing the underlying thermodynamics of the processes. Our comparative analysis of NRA performance across Cu surfaces underscores the pivotal role of pH in dictating intermediate free energies, particularly evident in acidic media where Cu(100) outperforms Cu(111) and Cu(110), with Na ions notably enhancing nitrate adsorption. Furthermore, our exploration of Ti_2CX_2 Mxenes with Cu attachments reveals promising prospects for enhanced NO_3^- adsorption, emphasizing the potential of functionalized surfaces to improve NRA efficiency compared to bare Cu surfaces.

The thermodynamic and kinetic complexities inherent in NRA pathways on Cu surfaces, especially in acidic and alkaline media, necessitate further investigation to fully unravel dominant reaction mechanisms and identify optimal surface configurations. Our findings underscore the need for continued research to refine our understanding of nitrate reduction on Cu surfaces and inform the design of more efficient catalytic systems for environmental remediation and sustainable nitrogen cycling.

REFERENCES

1. Smith, V.H., et al. (2019). Eutrophication: impacts of excess nutrient inputs on freshwater, marine, and terrestrial ecosystems. *Environmental Pollution*, 248, 453-462.
2. Ward, M.H., et al. (2018). Drinking water nitrate and human health: an updated review. *International Journal of Environmental Research and Public Health*, 15(7), 1557.
3. M. Duca, M. T. M Koper, et al. (2012). Powering denitrification: the perspectives of electrocatalytic nitrate to ammonia reduction. *Energy Environ. Sci.* 5, 9726-9742.
4. A. Thornton, P. Pearce, S. A. Parsons, et al. (2007). Ammonium removal from a solution using ion exchange on to MesoLite. *J. Hazard. Mater.* 147, 883-889.
5. Manoj Rayaroth, Charuvila Aravindakumar, Noor Shah, et al (2022). Advanced oxidation process (AOPs) based wastewater treatment – unexpected nitration side reactions – a serious environmental issue. *J. Chem Eng.* 430, 133002.
6. Yuting Wang, Yifu Yu, Ranran Jia, Chao Zhang, et al. (2019). Electrochemical synthesis of nitric acid from air and ammonia through waste utilization. *Natl. Sci. Rev.* 6, 730-738.
7. A.C.A. de Vooy, M.T.M. Koper, et al. (2001). Mechanistic study on the electrocatalytic reduction of nitric oxide on transition-metal electrodes, *J. Catal.* 202, 387–394.
8. G.E. Dima, A.C.A. de Vooy, M.T.M. Koper, et al. (2003). Electrocatalytic reduction of nitrate at low concentration on coinage and transition-metal electrodes in acid solutions, *J. Electroanal. Chem.* 554–555, 15–23.
9. I. Katsounaros, G. Kyriacou, et al. (2007). Influence of the concentration and the nature of the supporting electrolyte on the electrochemical reduction of nitrate on tin cathode. *Electrochim. Acta.* 52, 6412–6420.
10. R.R. Nazmutdinov, D.V. Glukhov, G.A. Tsirlina, O.A. Petrii, et al. (2005). Exploring the molecular features of cationic catalysis phenomenon: Peroxodisulfate reduction at a mercury electrode. *J. Electroanal. Chem.* 582, 118–129.
11. A. Manzo-Robledo, C. Lévy-Clément, N. Alonso-Vante, et al. (2014). The interplay between hydrogen evolution reaction and nitrate reduction on boron-doped diamond in aqueous solution: the effect of alkali cations. *Electrochim. Acta.* 117, 420–425.
12. Jin-Xun Liu, Danielle Richards, Nirala Singh, Bryan Goldsmith, et al. (2019). Activity and Selectivity trends in electrocatalytic nitrate reduction on transition metals. *ACS catal.* 9, 8, 7052-7064.

13. Tao Hu, Changhong Wang, Mengting Wang, Chang Ming Li, Chunxian Guo, et al. (2021). Theoretical insights into superior nitrate reduction to performance of copper catalysts. *ACS catal.* 11, 14417-14427.
14. Yuting Wang, et al. (2020). Unveiling the activity origin of a copper-based electrocatalyst for selective nitrate reduction to ammonia. *Angew. Chem. Int.* 59, 5350-5354.
15. Yian Wang, Xueping Qin, Minhua Shao, et al. (2021). First-principles mechanistic study on nitrate reduction reactions on copper surfaces: effects of crystal facets and pH. *Journal of Catalysis.* 400, 62-70.
16. Perdew, J. P. Burke, K. Ernzerhof, et al. (1996). Generalized Gradient Approximation Made Simple. *Phys. Rev. Lett.* 77, 3865–3868.
17. Kresse, G. Furthmuller, et al. (1996). Efficient Iterative Schemes for ab initio Total-energy. Calculations Using a Plane-wave Basis Set. *Phys. Rev.* 54, 11169–11186.
18. P.E. Blöchl, et al. (1994). Projector Augmented-wave Method. *Phys. Rev.* 50, 17953–17979.
19. H. J. Monkhorst, J. D. Pack, et al. (1976). Special Points for Brillouin-zone Integrations. *Phys. Rev.* 13, 5188–5192.
20. K. Mathew, R. Sundararaman, K. Letchworth-Weaver, T. A. Arias and R. G. Hennig, et al. (2014). Implicit solvation model for density functional study of nanocrystal surfaces and reaction pathways. *J. Chem. Phys.* 140, 084106.
21. S. Grimme, et al. (2006). Semiempirical GGA-type density functional constructed with a long-range dispersion correction. *J. Comput. Chem.* 27, 1787–1799.
22. W. Tang, E. Sanville and G. Henkelman, et al. (2009). A grid-based Bader analysis algorithm without lattice bias. *J. Phys. Condens. Matter.* 21, 084204.
23. V. Wang, N. Xu, J. C. Liu, G. and W. T. Geng, et al. (2019). *Comput. Phys. Commun.* 08269.
24. G. Henkelman, B. P. Uberuaga and H. Jónsson, et al. (2000). A climbing image nudged elastic band method for finding saddle points and minimum energy paths. *J. Chem. Phys.*, 2000, 113, 9901–9904.
25. S. E. Bae, K. L. Stewart, A. A. Gewirth, et al. (2007). Nitrate adsorption and reduction on Cu(100) in acidic solution. *J. Am. Chem. Soc.* 129, 10171–10180.
26. H. J. Wang, Q. Q. Mao, L. Wang, *ACS Appl. Mater. Interfaces*, 2021, 13, 44733–44741.

27. X. W. Zhai, H. X. Dong, Y. F. Li, X. D. Yang, L. Li, J. M. Yang, Y. W. Zhang, J. L. Zhang, H. X. Yan and G. X. Ge, *J. Colloid Interface Sci.*, 2021, 605, 897–905